JACS
JOURNAL OF THE AMERICAN CHEMICAL SOCIETY
Article
pubs.acs.org/JACS

New Insight into the Atomic-Scale Bulk and Surface Structure Evolution of $Li_4Ti_5O_{12}$ Anode

Xia Lu,[†,‡] Lin Gu,*[,†] Yong-Sheng Hu,[†] Hsien-Chieh Chiu,[‡] Hong Li,[†] George P. Demopoulos,*[,‡] and Liquan Chen[†]

[†]Beijing National Laboratory for Condensed Matter Physics, Institute of Physics, Chinese Academy of Sciences, Beijing 100190, China

[‡]Materials Engineering, McGill University, 3610 University Street, Montréal, Québec H3A 0C5, Canada

Supporting Information

ABSTRACT: Identifying the structure of electrodes at atomic-scale remains a key challenge but is a fertile realm for groundbreaking fundamental research in the advanced Li-ion battery material field. In this context, the subtle structure evolution taking place during lithiation/delithiation in the bulk/surface of $Li_4Ti_5O_{12}$ spinel (LTO) was probed using scanning transmission electron microscopy and found to undergo significant structure torque, namely Ti−O bond stretching/shrinking at different state-of-charge (SOC), which is not identified previously. This kind of nanostructure change plays an important role in facilitating the formation of capturing centers for the electron/hole pairs in a 3.80 eV insulating material as is LTO. Furthermore, with the aid of electron energy loss spectroscopy, the spontaneous charge transfer process, $Ti^{3+} \leftrightarrow e^- + Ti^{4+}$, was confirmed in the fully lithiated $Li_7Ti_5O_{12}$ surface as an essential step of the gas-releasing phenomenon. This new insight paves the way toward deeper comprehension and ultimately control of the electrochemical process for this and other important Li-ion battery materials.

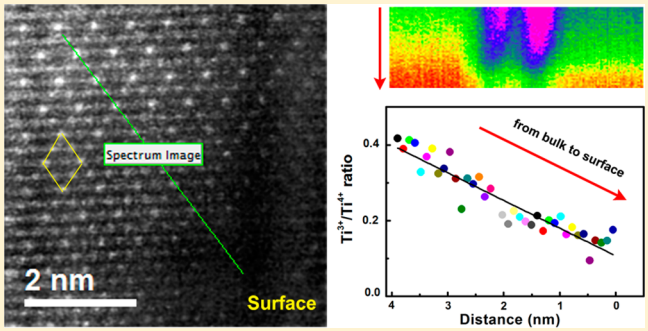

1. INTRODUCTION

Rechargeable Li-ion batteries have already been achieving great success in electric vehicles and large-scale energy storage beyond their dominating place with mobile devices. In the meantime, an increasing number of experimental and theoretical studies focusing on performance improvement and understanding, cycling life, and safety issues to make the batteries even better are continuously reported.[1−6] Due to its excellent electrochemical merits and structure stability upon cycling, $Li_4Ti_5O_{12}$ (LTO) spinel has been advocated as an important anode for long life and power Li-ion batteries (LIBs).[7−12] However, LTO is characterized by poor electronic conductivity on one hand and interfacial reactivity with the electrolyte on the other resulting in undesirable gas release that complicates the use of this important material in large-scale electrochemical energy storage applications.[13−17] Various modification techniques, including surface coating with carbon or metal oxides and formation of solid electrolyte interphase (SEI) layer have been advanced to improve LTO's conductivity and suppress its gas releasing reactivity.[18,19] The gas releasing issue remains however poorly understood and not fully resolved until now. This seems to indicate that the gas-releasing phenomena should be strongly related to the material's intrinsic properties of ionic/electronic storage and transport, especially in the surface structure and the solid−SEI−liquid interphase between the LTO electrode and the electrolyte. The reality is that the specific details on the structure evolution, especially the nanostructure distortions of LTO during the lithiation/delithiation process are far from being well understood and described, hence the undertaking of the present study.

Crystallographically, LTO spinel structure can be depicted as $Li[Li_{1/3}Ti_{5/3}]O_4$ with Li, $[Li_{1/3}Ti_{5/3}]$ and O, respectively, occupying the *8a*, *16d*, and *32e* sites.[7−9] During cycling, the *8a* site Li ions and the external Li ions insert into the empty *16c* sites causing the phase transition from the spinel LTO to the rock-salt $Li_7Ti_5O_{12}$ separated by an almost ideal heterointerface,[14,20] namely, two-phase reaction mechanism.[21] The energy barrier of ca. 0.3 eV as determined from first-principle calculations for internal Li ion migration from *8a* site to *16c* site, represents a relatively low activation energy that facilitates fast Li ion transport.[22,23] Macroscopically the "zero-strain" property characterized by high resolution in situ XRD patterns,[24] does not seem to be sensitive enough to describe its nanostructure evolution upon cycling. Recent results by Pang et al. demonstrated that the lattice of these anodes during continuous lithiation undergoes expansion followed by a gradual contraction and then expansion again; the measured lattice parameter changes were reconciled with Li occupation at

Received: November 10, 2014
Published: January 13, 2015

DOI: 10.1021/ja5115562
J. Am. Chem. Soc. 2015, 137, 1581−1586

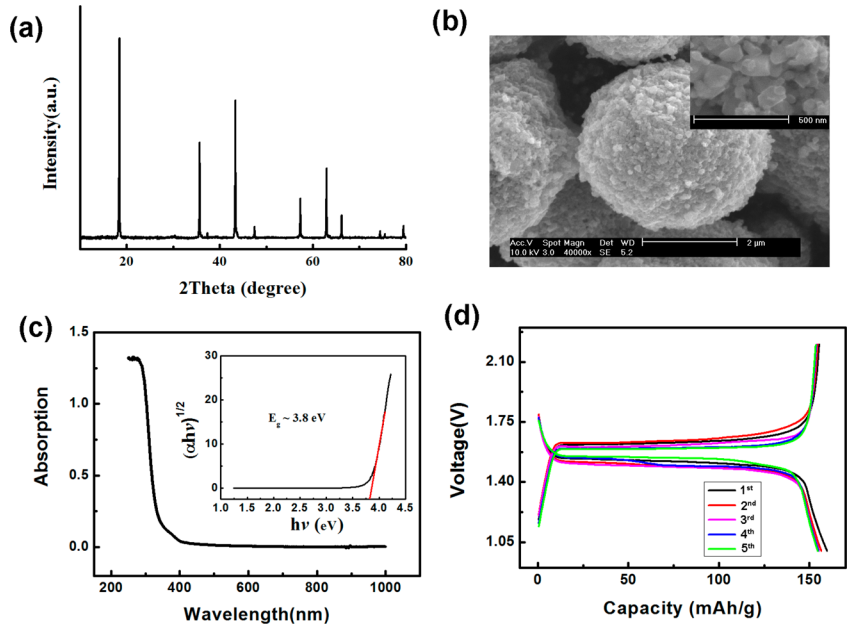

Figure 1. Structure and electrochemical performance characterization of the spherical $Li_4Ti_5O_{12}$ nanostructured materials. (a) XRD pattern, (b) SEM image with the magnified one in inset, (c) UV−vis absorption spectroscopy of the $Li_4Ti_5O_{12}$ sample with the wavelength ranging from 190 to 1000 nm; the calculated indirect optical band gap, 3.8 eV, is shown in the inset, and (d) electrochemical performance of first five cycles of $Li_4Ti_5O_{12}$ spheres at C/2 (1C = 175 mA/g) in a voltage range from 1.0 to 2.2 V.

specific sites within the LTO crystal structure using in situ neutron powder diffraction.[25] This means that the LTO electrode experiences structure changes in the process of accommodating Li. Despite of some recent work in this area,[14,26] the structure evolution in the bulk and the surface of LTO spinel remains unclear at atomic-scale.

Besides the confirmation of the Li ion storage sites and the two-phase reaction mechanism in our previous work, an abnormal surface was acquired from the lithiated LTO samples by spherical aberration-corrected scanning transmission electron microscopy techniques (STEM).[14] In particular the *16c* lattice sites were clearly occupied by heavy ions (here, it should be Ti ions) and exhibited a different surface configuration from that of the bulk in both STEM HAADF and ABF images. This result might be similar to the findings by Wang et al., who identified this surface layer as rutile-TiO_2.[26] However, as deduced from the projected LTO HAADF images, there may be alternative configurations with respect to occupation by *8a* Li ion, *16c* Li ion, *16d* Ti ion, and even the *16d* Li ion. Therefore, it is still difficult to shed light into the surface structure, notwithstanding the first-principle calculation results by Gao et al., according to which lithium-truncated surface is energetically beneficial in LTO spinel.[27] Furthermore, Borghols et al. reported that the near-surface environment of the nanosized LTO particles allows higher Li ion occupancies, leading to a larger storage capacity (simultaneous *8a* and *16c* occupation) and irreversible capacity loss, most likely due to surface reconstruction or mechanical failure.[28] So, it is critical to further probe the LTO nanostructure to unequivocally elucidate the ionic occupations and electron transfer mechanism and identify the intrinsic root causes of the gas-releasing issue. In this contribution, the STEM technique is employed (i) to demonstrate the bulk structure evolution on lithiated-$Li_4Ti_5O_{12}$ electrodes, (ii) to investigate the different surface structure states, and (iii) to explore the surface electronic charge distribution by electron energy loss spectroscopy (EELS). The results are highly important, not only clearly revealing the nanostructure transformations in the bulk but also characterizing the surface structure and the Ti^{3+}/Ti^{4+} distributions of lithiated LTO electrode.

2. EXPERIMENTAL SECTION

The cycling tests of LTO electrode were performed in an Swagelok-type cell between 3.0 and 0.5 V. A polypropylene film (Celgard 2300) was used as a separator. The working electrode was fabricated by casting the mixture of the active material, conductive agent (acetylene black: AB), and poly(vinylidene difluoride) (PVDF) in a weight ratio of ($Li_4Ti_5O_{12}$:AB:PVDF) 0.80:0.10:0.10 onto an aluminum foil. Metallic lithium foil was used as a counter electrode. The 1 M $LiPF_6$ in ethylene carbonate (EC) /dimethyl carbonate (DMC) (1:1 by volume) solvent was employed as electrolyte during the electrochemical tests.

After $Li_4Ti_5O_{12}$ samples were electrochemically lithiated, the cell was disassembled in the argon-filled glovebox. Then the lithiated $Li_4Ti_5O_{12}$ electrode was washed by a DMC solvent to remove the organic adsorbed components and dried in the vacuum chamber connected with glovebox. Finally, a small amount of powder was scratched from the electrode and dispersed in the DMC solvent. One droplet of the well-dispersed solution was spread onto the copper grid for STEM observation.

X-ray powder diffraction (XRD) patterns were recorded in the range of 10−80° using a Philips X'pert diffractometer with Bragg−Brentano geometry. The measurement was performed in a continuous scan mode, using Cu K_α X-ray source and a stepwidth of 0.0167°/s. A scanning electron microscope (SEM) (XL 30 S-FEG, FEI Co.) was used to study the sample morphology. The Ultra-Visible absorption spectroscopy of the sample was carried out on Cary 5000 spectrophotometer between 190 and 1100 nm. Aberration-corrected scanning transmission electron microscopy (STEM) and electron energy loss spectroscopy (EELS) was performed using a JEOL 2100F (JEOL, Tokyo, Japan) transmission electron microscope operated at 200 keV. The microscope is equipped with a CEOS (CEOS, Heidelberg, Germany) probe aberration corrector. The attainable spatial resolution of the microscope is 90 picometer at an incident semiangle of 20 mrad. To observe Li directly using an ABF collection

DOI: 10.1021/ja5115562
J. Am. Chem. Soc. 2015, 137, 1581−1586

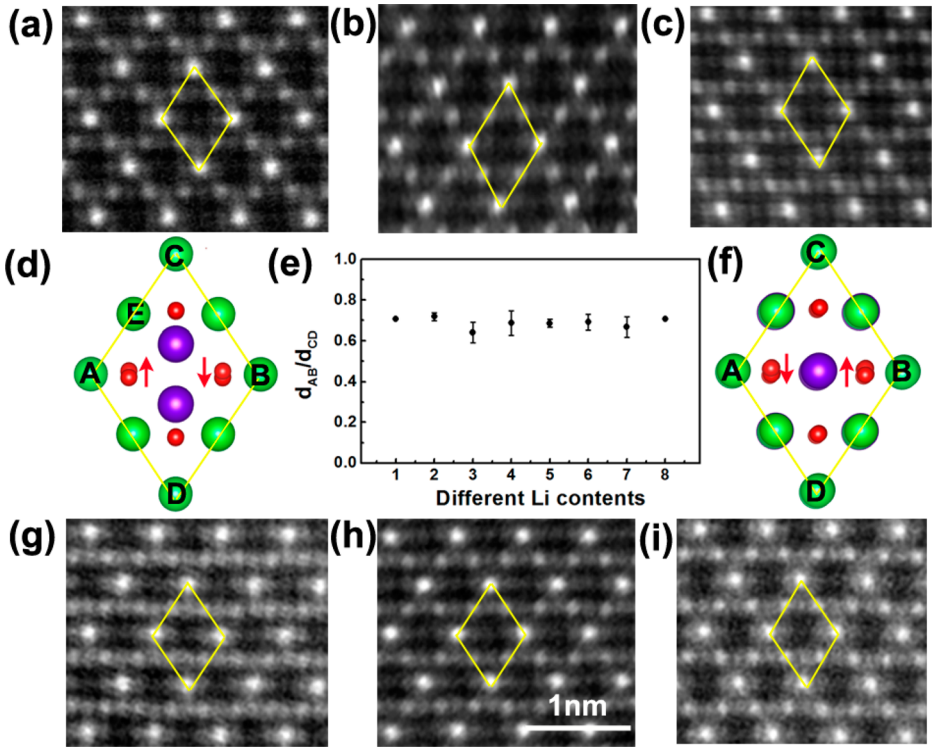

Figure 2. STEM-HAADF images and structure illustrations of $Li_4Ti_5O_{12}$ samples with different Li contents at [110] zone axis. (a) pristine, (b) half-charged, (c) charged to 3.0 V ($Li_4Ti_5O_{12}$), (d) and (f) schematic repeated units of $Li_4Ti_5O_{12}$ without/with lithiation (~3 Li per formula unit), (g) half-discharged, (h) discharged to 1.0 V ($Li_7Ti_5O_{12}$), (i) discharge to 0.5 V ($Li_{8.5}Ti_5O_{12}$ based on specific capacity) and (e) the numerical numbers from 1 to 8 correspond to the ratios of d_{AB}/d_{CD} in panels d, a, b, c, g, h, i, and f. In panels d and f, the green, the blue and red dots represent the Ti, Li, and O ionic occupations in $Li_4Ti_5O_{12}$ spinel structure. Additionally, from panel d and f there are two different Ti columns, namely Ti_A and Ti_E (different Ti contents), also two different O columns with one of them not fully overlapping with each other at [110] zone axis as appropriately indicated by the red arrows.

geometry, the acceptance semiangle was fixed between 10 and 20 mrad in this investigation.

3. RESULTS AND DISCUSSION

LTO spinel stacks in a cubic lattice with the edge-shared TiO_6 octahedra to constitute the fast Li ion transport framework. Supporting Information Figure S1 displays the LTO and $Li_7Ti_5O_{12}$ lattices viewed along [110] direction, the obvious difference from which lies in all interior *8a* site Li ions in LTO with the inserted Li ions migration into the *16c* sites in $Li_7Ti_5O_{12}$ lattice with subtle structure changes. Figure 1 demonstrates the as-prepared LTO microspheres obtained by the spray-drying method.[29] The sharp peaks and clean background of the XRD pattern of Figure 1a, indicate phase-pure and well-crystallized LTO samples, comprised of spherical agglomerates of 50 nm-sized primary particles (Figure 1b). In Figure 1c, the indirect optical band gap of ca. 3.80 eV is derived from the UV−vis. absorption spectroscopy on the white LTO powder using the empirical Urbach rule.[30−32] The interesting part is that the LTO despite its big band gap still demonstrates excellent high-rate perforemance, even for the naked powder, which necessitates a deeper understanding of its structural changes occurring during lithiation/delithiation and the associated charge (e^-) compensation and transport mechanisms. In Figure 1d, the LTO anode reversibly delivers ca. 160 mAh/g at 0.5 C in a votage range of 1.0−2.2 V with superior cycling performance as always. Then several LTO samples are intentionally prepared with different Li content, including the pristine, half-lithiated, fully lithiated ($Li_7Ti_5O_{12}$), over lithiated (discharged to 0.5 V), half-delithiated and fully delithited (charged to 3.0 V), which were used to characterize the structure evolution with the STEM as per procedural details published in previous studies.[14,33−36]

Supporting Information Figure S2 demonstrates an STEM-ABF image and corresponding line profile of the pristine LTO particle at [110] zone axis, from which the Li, Ti and O columns, even the Li storage mechansim, can be accurately acquired and identified with a series of ABF images on the basis of LTO spinel structure.[14] However, hereafter more attention is focused on the nanostructure evolution during lithiation/delithiation using the STEM-HAADF techniques, which is an effective way to image the Ti columns and the LTO spinel framework. The HAADF images of Figure 2 demonstrate a series of LTO structures with different Li contents at [110] zone axis. In Figure 2d and f, the repeated atomic structures of LTO and $Li_7Ti_5O_{12}$ are schematically denoted by the yellow quadrilateral ACBD, the characteristic difference between the two arising from the separate Li ion columns at this projected direction. The ratio of d_{AB}/d_{CD} is used to record the LTO nanostructure evolution and helps to eliminate errors by the STEM itself. Therefore, it provides an effective way to easily detect the subtle structure changes upon lithiation/delithiation. Here, it is determined to be about 0.708, with numbers "1" and "8" corresponding to the two end compositions for LTO and $Li_7Ti_5O_{12}$, respectively, as shown in Figure 2e. This value is a little smaller than the 0.718 value measured from the pristine LTO HAADF image in Figure 2a (number 2 in Figure 2e), which should be probably attributed to expansion as a result of

DOI: 10.1021/ja5115562
J. Am. Chem. Soc. 2015, 137, 1581−1586

the nanosize effect observed typically in such small LTO nanoparticles.

As it is shown in Figure 2e, upon lithiation the ratio d_{AB}/d_{CD} varies from the original 0.718 (pristine in Figure 2a: point 2), to 0.686 when half-lithiated (Figure 2g: point 5), to 0.691 when fully lithiated ($Li_7Ti_5O_{12}$ in Figure 2h: point 6) and finally to 0.669 when overlithiated (discharged to 0.5 V in Figure 2i: point 7), however with distinguishably increasing fluctuations. Upon delithiation, the d_{AB}/d_{CD} is seen to change from 0.691 when fully lithiated ($Li_7Ti_5O_{12}$ in Figure 2h: point 6) to 0.642 when half-delithiated (Figure 2b: point 3) and 0.688 when fully charged LTO (charged to 3.0 V in Figure 2c: point 4) with some irregular fluctuations. Furthermore, the different contrast of the O columns (red arrow in Figure 2d and f) can be clearly observed in one ABF image. These results reveal new solid evidence of nanoscale self-adjustment that plays a key role in accommodating Li insertion/extraction into/from the LTO spinel structure. As a matter of fact, there appears different phases to coexist in one lithitated LTO nanoparticle, including LTO, LTO/$Li_7Ti_5O_{12}$ interface, and $Li_7Ti_5O_{12}$,[14] in addition to separated LTO and $Li_7Ti_5O_{12}$ nanoparticles during cycling,[37] all of which contribute a lot to the fluctuating d_{AB}/d_{CD} values. Fundamentally, this fluctuation reflects the stretch/shrink of the crystallographic Ti−O−Ti bonds in LTO structure. This kind of Ti−O bond stretch/shrink is supposed to reversibly introduce electron/hole trapping centers (Ti^{3+}/Ti^{4+}),[38,39] which play a key role in facilitating charge carrier (e^-) migration in such a big band gap material. Consequently, the observed structure distortion (electron/polaron) has as result to lower the energy barrier for quick electron hopping without adversely influencing Li ion transport through the spinel lattice hence endowing LTO with superior cycling performance.

Figure 3 presents different surface structures of spherical LTO particles as revealed by STEM-HAADF imaging. Considering the evolution of the surface quadrilateral ACBD, the lengths of d_{AB} and d_{CD} are found to be about 115% larger in the (110) surface than in the bulk (Figure 3a); at the same time they are ca. 150% larger in the (111) plane of the topmost surface layers than the corresponding ones in the bulk (Figure 3c). (Here, the ratio of 115% and 150% are statistically average results measured over different surface regions in various STEM images.) This apparently means that the LTO surface experiences structure relaxation in the surface region, even surface reconstruction as evident in Figure 3b with respect to the bulk structure in Figure 2a. Moreover as deduced from Supporting Information Figure S6, the clear $\sum 3$ twin boundary is characterized with unambiguous strain distribution in the (111) plane. Hence, it can be seen that the surface is far below than "perfect" in LTO nanocrystals. Then according to Figure 3b there should be no atomic contrast detected in the Li *16c* site of the pristine LTO STEM-HAADF image, however electron energy loss spectroscopy (EELS) revealed rather bright atomic occupation of Ti columns as discussed later in Figure 4a, that is, the surface relaxation induces the *16d* Ti ions to move to the *16c* Li ions lattice sites creating some abnormal surface Ti−O coordinations with respect to the bulk. Obviously, there exists some Li−Ti column overlapping in the surface region (~1.7 nm topmost layer). Occasionally a similar disordered surface region can be found using a high energy electron nanobeam to puncture (burn) the bulk area as shown in Supporting Information Figure S4. Likewise, this kind of Ti−O disordered coordinations can be found in the (001) Ti-terminated surface region of perovskite $SrTiO_3$[40] and a similar reconstructed surface structure can be observed in cycled $LiMn_2O_4$ spinel cathode.[41] It might be inferred therefore that the reconstructed LTO surface seems to be the most energetically favorable configuration. Because the HAADF image represents a combination of viewing edge directions that cannot be discerned from the projection alone, it is difficult to extract any further information from imaging alone. We propose that this kind of reconstructed LTO surface plays a key role in enabling good Li ion and electron ($Li^+ + e^-$) transport properties acting as de facto conducting coating on the regular LTO particles hence affecting the local electrochemical environment, which translates to capacity increase in some cases.[28]

In addition to the surface relaxation and reconstruction as described above, the surface dangling bonds serve as improtant electrochemically active centers during the cycling of LTO. Thus, as shown in Figure 3 and Supporting Information Figure S5, they have a large number of Ti columns, possibly the unsaturated Ti−O bonds, that are terminated on the LTO (110), (111) as well as the less common (121) surfaces, with which the moisture and CO_2 can be absorbed when exposed in air. Hence, this kind of Ti (or Ti−O) terminations are prone to Ti−O: R ligand attachments, where R could be Li^+, H^+, CH_3^+, and other organic radicals. As a result of this type of ligand attachments, the symmetric TiO_6 octahedron would break down irreversibly causing stretching/shrinking of the Ti−O bonds and formation of the electron/hole capturing centers, which are mainly responsible for the package swelling issue exhibited by LTO electrodes.[17] Therefore, a number of changes is seen to occur on the LTO surface, including the surface relaxation, the Li−Ti overlap along [110] directions, the possible Ti−O: R ligand attachments and the exposure of the electrochemically active isolated Ti centers (Supporting Information Figure S5), all of which can have a bearing upon the lithiation/delithiation process. Beyond the identification of all these subtle changes, the specific molecular reaction

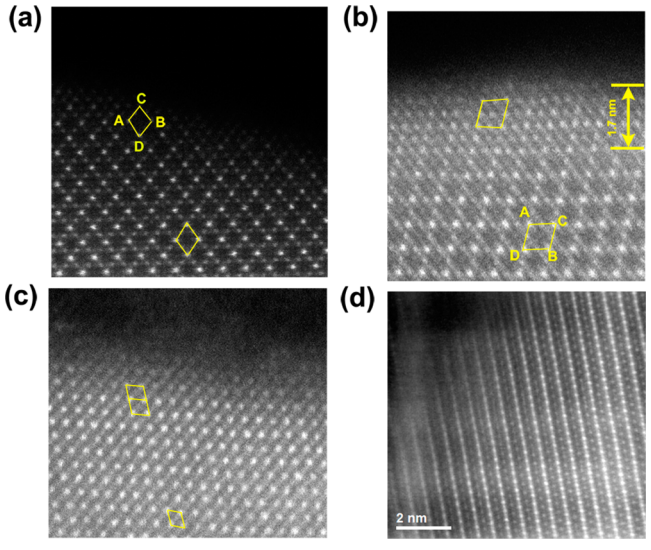

Figure 3. Images of atomic-scale surface structures of $Li_4Ti_5O_{12}$ samples obtained with STEM-HAADF techniques. (a) Clean (110) surface, (b) (110) surface with obvious Li−Ti disorders in the *8a* site, (c) (111) and (d) (121) surfaces. The corresponding sructure illustrations are provided in Supporting Information Figure S3. A $\sum 3$ twin boundary is also acquired in the (111) plane as shown in Supporting Information Figure S6.

DOI: 10.1021/ja5115562
J. Am. Chem. Soc. 2015, 137, 1581−1586

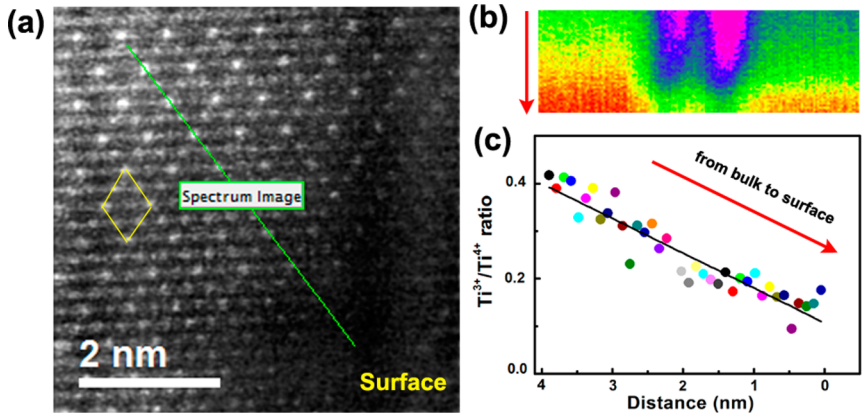

Figure 4. Electron energy loss spectroscopy (EELS) profiles on $Li_7Ti_5O_{12}$ (110) surface. (a) Line-scanning EELS trajectory from bulk to surface on the (110) plane, (b) the collected EELS spectra, and (c) the corresponding Ti^{3+}/Ti^{4+} cation ratio profile derived from the EELS spectra in panel b. The specific fitting process is described in Supporting Information Figure S7.

mechanism responsible for the gas-releasing problem needs to be further elucidated for LTO electrode in future.

Next electron energy loss spectroscopy (EELS) was employed to detect the charge distributions on the fully lithiated LTO ($Li_7Ti_5O_{12}$) (110) surface as shown in Figure 4. As shown in Figure 4b, a series of legible EELS on the Ti columns are acquired from (110) bulk region to the surface region (Figure 4a). (Note that the high energy resolution in Figure 4b is at the cost of spatial resolution. However, the basic repeated units (ACBD) are still distinguishable.) Then using the standard Ti^{3+} (Supporting Information Figure S7b) and Ti^{4+} (Supporting Information Figure S7c) EELS to fit the acquired EELS in the surface region as shown in Figure 4b (fitting detials are provided in Supporting Information Figure S7), the quantitative ratio of Ti^{3+}/Ti^{4+} can be derived for each acquired Ti column as shown in Figure 4c. Figure 4c reveals that the Ti^{3+}/Ti^{4+} ratio decreases steeply from the bulk to the surface region approaching zero at the outermost surface layers in this fully lithiated LTO sample. During normal lithiation of LTO as generallized by the reaction $Li^+ + e^- + Ti^{4+} \rightarrow Li^+ + Ti^{3+}$, all the interior *8a* Li ions and the inserted Li ions migrate ino the *16c* sites to form the rock-salt $Li_7Ti_5O_{12}$ phase.[14] However, according to our EELS results at the outermost surface region besides normal lithiation, the reverse reaction of $Li^+ + Ti^{3+} \rightarrow Li^+ + e^- + Ti^{4+}$ can be inferred from the near to zero Ti^{3+}/Ti^{4+} ratio to occur, which means that the tetravalent state of the electrochemically active Ti center is spontaneously maintained. The electron (e^-) relased by the surface Ti^{3+}/Ti^{4+} change can be further involved in oxidizing/reducing the organic molecules (even radicals or lithium salts) in the electrolyte and the solid-SEI-electrolyte interface. Therefore, it is proposed that the spontaneous reversible surface reaction $Ti^{3+} \leftrightarrow e^- + Ti^{4+}$ occurring in the fully lithiated LTO to play a key role in the gas releasing phenomenon.

4. CONCLUSION

In summary, $Li_4Ti_5O_{12}$ spheres were employed as Li-ion battery anode and their bulk/surface structure changes during lithiation were carefully investigated at atomic-scale using spherical aberration-corrected scanning transmission electron microscopy techniques. Based on the STEM-HAADF observations, the $Li_4Ti_5O_{12}$ anode experiences remarkable nanostructure evolution at different Li content levels (i.e., different states-of-charge, SOC). In particular, we found LTO to undergo significant structure torque, namely, Ti−O bond stretching/shrinking at different SOCs, which is instrumental in dynamically establishing the capturing centers for electron/hole pairs. Consequently, these irregular capturing centers are thought to facilitate electron (e^-) hopping effectively overcoming the large energy barrier (roughly the 3.8 eV optical band gap). However, they have no adverse effect on Li ion transport and storage properties as macroscopically LTO's cubic phase remains unchanged upon lithiation into ($Li_7Ti_5O_{12}$), for which its known as "zero-strain" material.

Further our electron energy loss spectroscopy investigation reveals that the Ti^{3+}/Ti^{4+} ratio decreases steeply from the bulk to the surface region approaching zero at the outermost surface layers of the fully lithiated LTO. It was concluded that there is a reversible spontaneous surface reaction of $Ti^{3+} \leftrightarrow e^- + Ti^{4+}$ occurring on the surface (ordered or disordered) of lithiated $Li_4Ti_5O_{12}$ that potentially plays a key role in the gas releasing phenomenon but further works needed to confirm this connection.

These findings shed new light on the atomic scale structure and charge transport mechanism prevailing during lithiation of $Li_4Ti_5O_{12}$ anode and clearly distinguishing the drastic differences in bulk and surface phenomena that need to be fully comprehended and ultimately controlled.

■ ASSOCIATED CONTENT

Ⓢ Supporting Information

The $Li_4Ti_5O_{12}$ and $Li_7Ti_5O_{12}$ lattice, the STEM-ABF image of $Li_4Ti_5O_{12}$, the illustrations of the $Li_4Ti_5O_{12}$ (110), (111), and (121) surfaces, the artificial $Li_4Ti_5O_{12}$ surface and HAADF image with dangling Ti−O bonds, the observed $\sum 3$ Twin boundary and the details for the fitting to EELS spectra acquired from the $Li_7Ti_5O_{12}$ surface. This material is available free of charge via the Internet at http://pubs.acs.org.

■ AUTHOR INFORMATION

Corresponding Authors

l.gu@iphy.ac.cn
george.demopoulos@mcgill.ca

Notes

The authors declare no competing financial interest.

DOI: 10.1021/ja5115562
J. Am. Chem. Soc. 2015, 137, 1581−1586

■ ACKNOWLEDGMENTS

This work was supported with funding from the "973" Projects (2010CB833102, 2012CB932900), NSFC (51222210, 11234013, 11174334), State Grid Corporation of China "$Li_4Ti_5O_{12}$ based stationary battery and system" Project, "Strategic Priority Research Program" of the Chinese Academy of Sciences (Grant No. XDA01020304) and One Hundred Talent Project of the Chinese Academy of Sciences) as well as the Natural Sciences & Engineering Research Council of Canada (NSERC).

■ REFERENCES

(1) Tarascon, J. M.; Armand, M. *Nature* **2001**, *414* (6861), 359−367.
(2) Bruce, P. G.; Scrosati, B.; Tarascon, J. M. *Angew. Chem., Int. Ed.* **2008**, *47* (16), 2930−2946.
(3) Armand, M.; Tarascon, J. M. *Nature* **2008**, *451* (7179), 652−657.
(4) Li, H.; Wang, Z. X.; Chen, L. Q.; Huang, X. J. *Adv. Mater.* **2009**, *21* (45), 4593−4607.
(5) Goodenough, J. B.; Kim, Y. *Chem. Mater.* **2010**, *22* (3), 587−603.
(6) Zu, C. X.; Li, H. *Energy Environ. Sci.* **2011**, *4* (8), 2614−2624.
(7) Deschanv, A.; Raveau, B.; Sekkal, Z. *Mater. Res. Bull.* **1971**, *6* (8), 699−704.
(8) Ferg, E.; Gummow, R. J.; Dekock, A.; Thackeray, M. M. *J. Electrochem. Soc.* **1994**, *141* (11), L147−L150.
(9) Ohzuku, T.; Ueda, A.; Yamamoto, N. *J. Electrochem. Soc.* **1995**, *142* (5), 1431−1435.
(10) Zhao, L.; Hu, Y. S.; Li, H.; Wang, Z. X.; Chen, L. Q. *Adv. Mater.* **2011**, *23* (11), 1385−1388.
(11) Zaghib, K.; Simoneau, M.; Armand, M.; Gauthier, M. *J. Power Sources* **1999**, *81*, 300−305.
(12) Chiu, H. C.; Brodusch, N.; Gauvin, R.; Guerfi, A.; Zaghib, K.; Demopoulos, G. P. *J. Electrochem. Soc.* **2013**, *160* (5), A3041−A3047.
(13) Du Pasquier, A.; Plitz, I.; Menocal, S.; Amatucci, G. *J. Power Sources* **2003**, *115* (1), 171−178.
(14) Lu, X.; Zhao, L.; He, X. Q.; Xiao, R. J.; Gu, L.; Hu, Y. S.; Li, H.; Wang, Z. X.; Duan, X. F.; Chen, L. Q.; Maier, J.; Ikuhara, Y. *Adv. Mater.* **2012**, *24* (24), 3233−3238.
(15) He, Y. B.; Li, B. H.; Liu, M.; Zhang, C.; Lv, W.; Yang, C.; Li, J.; Du, H. D.; Zhang, B. A.; Yang, Q. H.; Kim, J. K.; Kang, F. Y. *Sci. Rep.* **2012**, *2*, 913.
(16) Belharouak, I.; Koenig, G. M.; Tan, T.; Yumoto, H.; Ota, N.; Amine, K. *J. Electrochem. Soc.* **2012**, *159* (8), A1165−A1170.
(17) Wu, K.; Yang, J.; Zhang, Y.; Wang, C. Y.; Wang, D. Y. *J. Appl. Electrochem.* **2012**, *42* (12), 989−995.
(18) Kitta, M.; Akita, T.; Maeda, Y.; Kohyama, M. *Langmuir* **2012**, *28* (33), 12384−12392.
(19) He, Y. B.; Liu, M.; Huang, Z. D.; Zhang, B.; Yu, Y.; Li, B. H.; Kang, F. Y.; Kim, J. K. *J. Power Sources* **2013**, *239*, 269−276.
(20) Tanaka, S.; Kitta, M.; Tamura, T.; Maeda, Y.; Akita, T.; Kohyama, M. *J. Mater. Sci.* **2014**, *49* (11), 4032−4037.
(21) Kitta, M.; Akita, T.; Tanaka, S.; Kohyama, M. *J. Power Sources* **2013**, *237*, 26−32.
(22) Chen, Y. C.; Ouyang, C. Y.; Song, L. J.; Sun, Z. L. *Electrochim. Acta* **2011**, *56* (17), 6084−6088.
(23) Sun, Y.; Zhao, L.; Pan, H. L.; Lu, X.; Gu, L.; Hu, Y. S.; Li, H.; Armand, M.; Ikuhara, Y.; Chen, L. Q.; Huang, X. J. *Nat. Commun.* **2013**, *4*, 1870.
(24) Ronci, F.; Reale, P.; Scrosati, B.; Panero, S.; Albertini, V. R.; Perfetti, P.; di Michiel, M.; Merino, J. M. *J. Phys. Chem. B* **2002**, *106* (12), 3082−3086.
(25) Pang, W. K.; Peterson, V. K.; Sharma, N.; Shiu, J. J.; Wu, S. H. *Chem. Mater.* **2014**, *26* (7), 2318−2326.
(26) Wang, Y. Q.; Guo, L.; Guo, Y. G.; Li, H.; He, X. Q.; Tsukimoto, S.; Ikuhara, Y.; Wan, L. J. *J. Am. Chem. Soc.* **2012**, *134* (18), 7874−7879.
(27) Gao, Y. R.; Wang, Z. X.; Chen, L. Q. *J. Power Sources* **2014**, *245*, 684−690.
(28) Borghols, W. J. H.; Wagemaker, M.; Lafont, U.; Kelder, E. M.; Mulder, F. M. *J. Am. Chem. Soc.* **2009**, *131* (49), 17786−17792.
(29) Wen, Z. Y.; Gu, Z. H.; Huang, S. H.; Yang, J. H.; Lin, Z. X.; Yamamoto, O. *J. Power Sources* **2005**, *146* (1−2), 670−673.
(30) Tauc, J.; Grigorov, R.; Vancu, A. *Phys. Status Solidi* **1966**, *15* (2), 627−637.
(31) Davydov, A. S. *Phys. Status Solidi B* **1968**, *27* (1), 51−56.
(32) Lu, X.; Jian, Z. L.; Fang, Z.; Gu, L.; Hu, Y. S.; Chen, W.; Wang, Z. X.; Chen, L. Q. *Energy Environ. Sci.* **2011**, *4* (8), 2638−2644.
(33) Gu, L.; Zhu, C. B.; Li, H.; Yu, Y.; Li, C. L.; Tsukimoto, S.; Maier, J.; Ikuhara, Y. *J. Am. Chem. Soc.* **2011**, *133* (13), 4661−4663.
(34) Lu, X.; Sun, Y.; Jian, Z. L.; He, X. Q.; Gu, L.; Hu, Y. S.; Li, H.; Wang, Z. X.; Chen, W.; Duan, X. F.; Chen, L. Q.; Maier, J.; Tsukimoto, S.; Ikuhara, Y. *Nano Lett.* **2012**, *12* (12), 6192−6197.
(35) Suo, L. M.; Han, W. Z.; Lu, X.; Gu, L.; Hu, Y. S.; Li, H.; Chen, D. F.; Chen, L. Q.; Tsukimoto, S.; Ikuhara, Y. *Phys. Chem. Chem. Phys.* **2012**, *14* (16), 5363−5367.
(36) Lu, X.; Wang, Y.; Liu, P.; Gu, L.; Hu, Y.-S.; Li, H.; Demopoulos, G. P.; Chen, L. *Phys. Chem. Chem. Phys.* **2014**, *16* (40), 21946−21952.
(37) Wagemaker, M.; Simon, D. R.; Kelder, E. M.; Schoonman, J.; Ringpfeil, C.; Haake, U.; Lutzenkirchen-Hecht, D.; Frahm, R.; Mulder, F. M. *Adv. Mater.* **2006**, *18* (23), 3169−3173.
(38) Di Valentin, C.; Pacchioni, G.; Selloni, A. *Phys. Rev. Lett.* **2006**, *97* (16), 166803.
(39) Angelis, F. D.; Valentin, C. D.; Fantacci, S.; Vittadini, A.; Selloni, A. *Chem. Rev.* **2014**, *114* (19), 9708−9753.
(40) Zhu, G. Z.; Radtke, G.; Botton, G. A. *Nature* **2012**, *490* (7420), 384−387.
(41) Tang, D. C.; Sun, Y.; Yang, Z. Z.; Ben, L. B.; Gu, L.; Huang, X. J. *Chem. Mater.* **2014**, *26* (11), 3535−3543.

DOI: 10.1021/ja5115562
J. Am. Chem. Soc. 2015, 137, 1581−1586